Int. J. Multiphase Flow Vol. 19, No. 5, pp. 737–749, 1993
Printed in Great Britain.

0301-9322/93 $6.00 + 0.00

SHOCK WAVE/BOUNDARY LAYER INTERACTION WITH HEAT ADDITION BY NONEQUILIBRIUM PHASE TRANSITION

G. H. SCHNERR and P. Li
Institut für Strömungslehre und Strömungsmaschinen, Universität Karlsruhe (TH), 76128 Karlsruhe, Germany

(Received 29 July 1992; in revised form 15 June 1993)

Abstract—This investigation deals with the interaction of a turbulent boundary layer and a normal shock wave caused by supercritical heat addition in homogeneously condensing flows. The method used is a combination of analytical and numerical procedures, which is based on the perturbation method of Bohning & Zierep for the shock/boundary layer interaction in adiabatic flow. The homogeneous condensation process is described by the classical nucleation theory of Volmer together with the molecular droplet growth law of Hertz and Knudsen. The cooling rate, the nucleation rate, the surface-averaged droplet radius and the condensate mass fraction are analyzed along several streamlines in the boundary layer. The strength of the shock wave caused by supercritical heat addition in the outer flow field weakens and ultimately vanishes near the boundary edge by the influence of viscous effects. Comparison is made of the integral boundary layer variables and the friction coefficient in adiabatic flow with those in diabatic flow.

Key Words: turbulent boundary layer, nucleation, droplet growth, shock interaction

INTRODUCTION

Stationary 2-D flow of vapor/carrier gas mixtures (moist air) with nonequilibrium homogeneous condensation has been investigated extensively in theory and experiment by Schnerr (1986, 1989, 1993), Dohrmann (1989), Schnerr & Dohrmann (1990) and Wegener (1987, 1991). A mathematical theory for the critical amount of heat leading to thermal choking and the formation of normal shocks in 1-D nozzle flows has been presented recently by Delale *et al.* (1993). In this work a cubic equation for an estimate of the limiting condensate mass fraction in shock-free condensing nozzle flows was derived, and a criterion for the existence of supercritical condensing flows has been established. It has been shown that the flow Mach number at thermal choking is not necessarily unity in condensing nozzle flows, due to the variation from the temperature dependence on the latent heat. Particular aspects of compressible flows with heat addition near Mach number unity are detailed in Zierep (1971, 1974). Viscous flows including homogeneous condensation and evaporation were investigated theoretically by Studzinsky (1979) and Ryley (1971), using simplified models for the description of the processes of condensation and evaporation within the boundary layer. Transonic turbulent boundary layers with homogeneous condensation were investigated numerically for the first time by Jantzen (1990) and Schnerr *et al.* (1992) using analytical and numerical methods which combine the classical nucleation theory and the Hertz–Knudsen droplet growth law with a compressible boundary layer algorithm. In their work only the boundary layer flow with subcritical heat addition by homogeneous condensation was considered. In the present work we investigate the shock/boundary layer interaction with supercritical heat addition by nonequilibrium phase transition in Laval nozzle flows. A region of thickness δ_0 (thickness of the oncoming boundary layer) beginning in front of the shock far upstream of the condensation onset and ending behind the nonequilibrium heat release is defined as the shock/boundary layer interference area and the nozzle walls are taken to be adiabatic.

METHOD OF CALCULATION

The method of calculation is a combination of analytical and numerical procedures for the shock/boundary layer interaction together with the description of the homogeneous condensation process by the classical nucleation theory and the Hertz–Knudsen droplet growth law.

Calculation of the Shock/Boundary Layer Interaction

The calculation of the shock/boundary layer interference area is based on the analytical model of Bohning & Zierep (1976) and Bohning (1982). The boundary layer is subdivided into a shear layer and a sublayer with fully active viscous effects close to the wall (Lighthill 1961). The equations of mass, momentum and energy and the equation of state lead to the following perturbed system:

$$\varrho_B \frac{\partial u_d}{\partial x} + \frac{\partial(\varrho_B v_d)}{\partial y} + M_B^* \frac{\partial \varrho_d}{\partial x} = 0, \quad [1]$$

$$\varrho_B M_B^* \frac{\partial u_d}{\partial x} + \varrho_B v_d \frac{dM_B^*}{dy} = -\frac{1}{\gamma}\frac{\partial p_d}{\partial x} + \frac{1}{Re_\delta}\cdot\frac{\partial^2 u_d}{\partial y^2}, \quad [2]$$

$$\varrho_B M_B^* \frac{\partial v_d}{\partial x} = -\frac{1}{\gamma}\frac{\partial p_d}{\partial y}, \quad [3]$$

$$T_d + (\gamma - 1)M_B^* u_d = q \quad [4]$$

and

$$\varrho_B T_d + \varrho_d T_B = p_d. \quad [5]$$

This is a system of linearized differential equations for the disturbance quantities "d", which is valid in the whole boundary layer. The subscript "B" marks the basic flow field whose turbulent velocity profile is approximated by the exponential function

$$M_B^*(y) = y^\beta. \quad [6]$$

Here all physical variables (density ϱ, pressure p, temperature T and Cartesian velocity components u and v) are made dimensionless by the corresponding critical values of the inviscid flow, and the coordinates x and y by the thickness (δ_0) of the oncoming boundary layer. The Reynolds number is defined by $Re_\delta = c^* \cdot \delta/\nu$ and the heat addition as $q = Q/(c_p T^*)$. M^* is the critical Mach number and γ is the specific heat ratio. The interference area is taken as a rectangle of thickness δ_0 and the boundary conditions required for the analytical calculation are shown in figure 1.

For the computation of disturbances in the compressible shear layer the viscous term in [2] plays a subordinate role. On the assumption that this term is neglected, and with the definitions

$$p_d \equiv -\gamma\frac{\partial\phi}{\partial x}, \quad v_d \equiv \frac{M_B^*(y)}{M_B^2(y)}\frac{\partial\phi}{\partial y}, \quad [7]$$

the system [1]–[5] reduces to a single differential equation for the function $\phi(x, y)$:

$$\phi_{yy} - \frac{2}{M_B}\frac{dM_B}{dy}\phi_y + (1 - M_B^2)\phi_{xx} = \varrho_B M_B^2 \frac{\partial q}{\partial x}. \quad [8]$$

Transformation of the boundary conditions according to [7] yields an elliptical boundary value problem with parabolic edge at $y = 1$. Equation [8] is solved analytically using separation of variables.

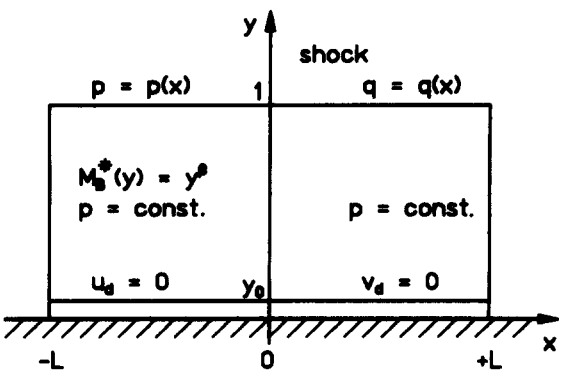

Figure 1. Boundary conditions of the disturbance problem.

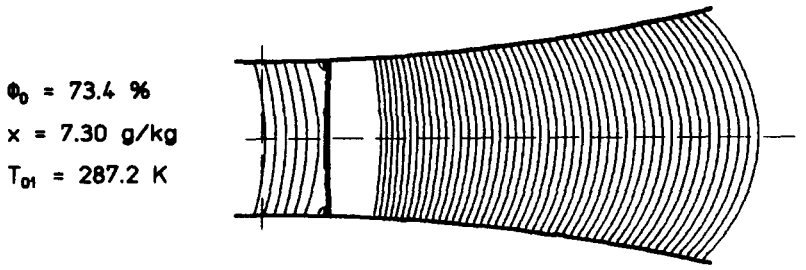

Figure 2. Supercritical heat addition by homogeneous condensation in a circular-arc nozzle; $2y^* = 30$ mm, $R^* = 400$ mm, temperature gradient $(dT/dx)^* = -8.04°C/cm$, flow from left. Supersonic frozen iso-Mach lines are plotted.

The thickness of the sublayer close to the wall can be calculated from Re_δ and the shape factor of the undisturbed velocity profile (Bohning 1982):

$$y_0 = 1.14 \cdot \left(\frac{1}{Re_\delta}\right)^{\frac{1}{2+\beta}}. \qquad [9]$$

In the subsequent calculations Re_δ at the inflow of the interference area and β are taken to be 10,000 and 1/7, respectively. In this analytical solution the x-dependence of the basic flow field is neglected and the extension of the shock/boundary layer interference region in the x-direction is restricted to a small distance.

In order to remove the restrictions of the analytical solution, the tangential component of the velocity is calculated by numerically solving the Navier–Stokes momentum equation in the streamwise direction (Breitling 1989). The algorithm follows the implicit scheme of Beam & Warming (1978) combined with the two-layer turbulence model of Cebeci & Smith (1974). Density, static pressure and the normal component of the velocity with correction are given as coefficients from the analytical solution. As an additional boundary condition solving the momentum equation $u_{xx} = 0$ is used at the outflow boundary.

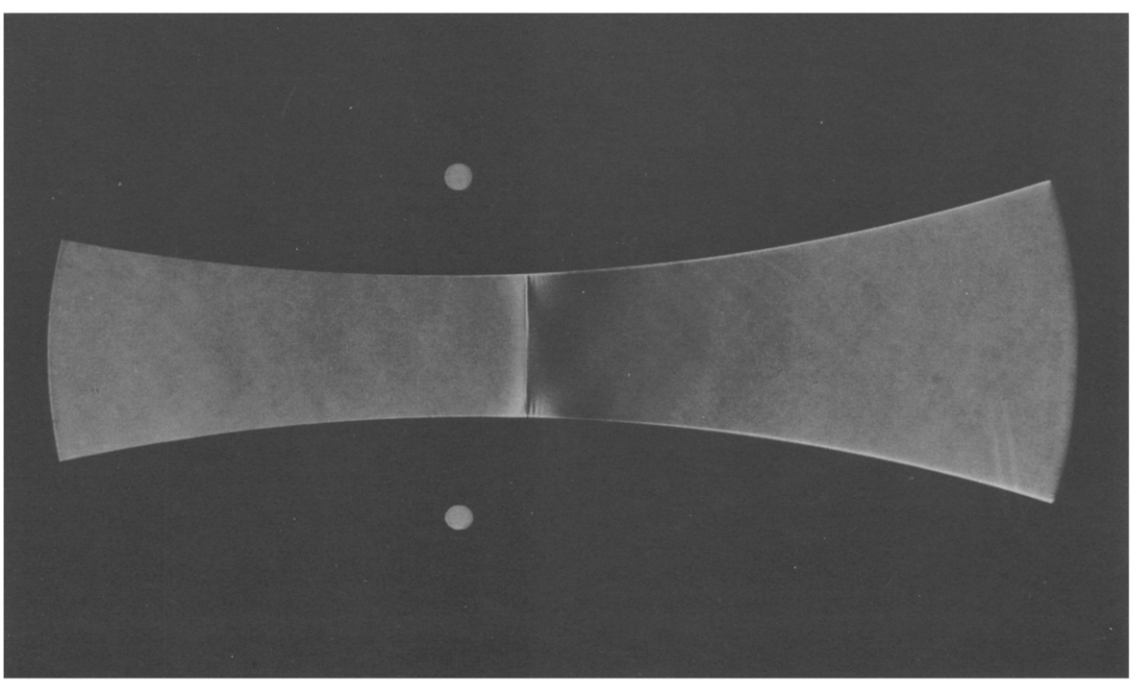

Figure 3. Schlieren picture with supercritical heat addition; $\phi_0 = 73.4\%$, mixing ratio $x = 7.3$ g/kg, $T_{01} = 287.2$ K, flow from left.

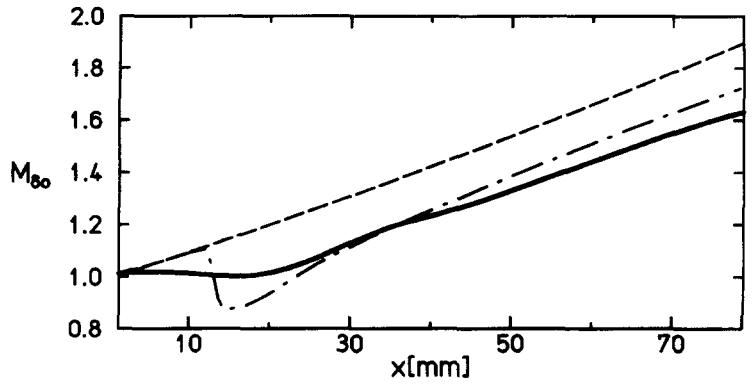

Figure 4. Adiabatic (- - -), diabatic (——) M at the upper edge of the interference area and diabatic (- · -) M in the outer flow field; sidewall–circular-arc nozzle axis.

Evaluation of Homogeneous Condensation

The rate of heat addition by nonequilibrium phase transition is calculated along different streamlines in the boundary layer. The classical nucleation theory of Volmer (1939) is used to calculate the nucleation rate:

$$J = \sqrt{\frac{2}{\pi}}\sqrt{\sigma_\infty}\, m^{-1.5}\frac{\varrho_v^2}{\varrho_c}\exp\left[-\frac{16}{3}\pi\frac{\sigma_\infty^3}{m\varrho_c^2 R_v^3 T^3 \ln^2(S)}Y\right]. \qquad [10]$$

Herein σ_∞, S, ϱ_v and ϱ_c denote surface tension, saturation ratio, density of vapor and of condensate. R_v is the specific gas constant of the vapor and m the mass per molecule. For liquid condensate we have $Y = 1$. With the assumption of solid condensate, the factor Y after Yang (Dohrmann 1989) which corrects for the Brownian motion of the molecules is introduced as

$$Y = 1 + 2\left[\frac{2}{n^*} - \left(\frac{2}{n^*}\right)^{2/3}\right], \qquad [11]$$

with n^* as the number of molecules of a critical nucleus with radius r^*. The microscopic droplet growth is described by the Hertz–Knudsen formula as

$$\frac{dr}{dt} = \frac{\alpha}{\rho_c}\frac{p_v - p_{s,r}}{\sqrt{2\pi R_v T}}; \qquad [12]$$

p_v and $p_{s,r}$ are the pressure of the vapor and the saturation pressure of the droplet with radius r, respectively. Additional empirical relationships from experiments (Schnerr & Dohrmann 1990) are

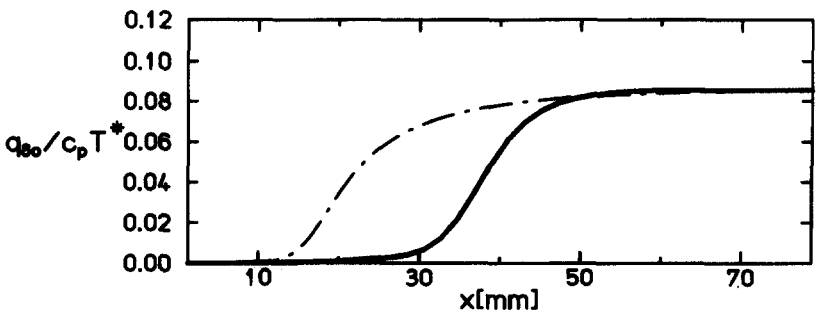

Figure 5. Heat addition from homogeneous condensation at the upper edge of the interference area (——) and in the outer flow field (- · -); sidewall–circular-arc nozzle axis.

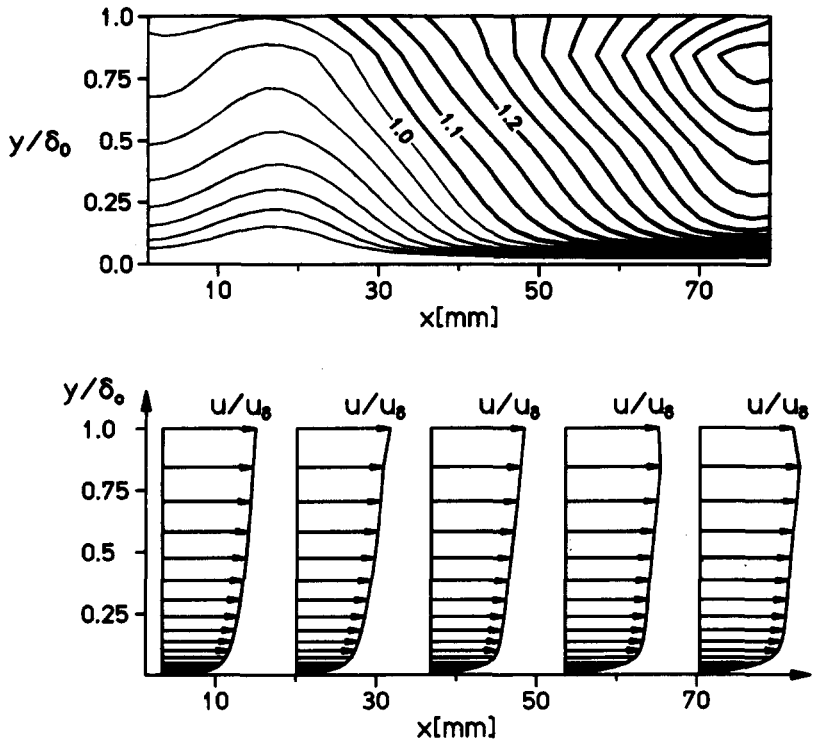

Figure 6. M contours (increment $\Delta M = 0.05$) and velocity profiles inside the boundary layer; sidewall–circular-arc nozzle axis.

necessary for the unknown surface tension and condensation coefficient α, which is set to unity for the liquid condensate and 0.2 for ice. For the condensate mass fraction g we have

$$\frac{dg}{dt} = \frac{4}{3}\pi r^{*3}\varrho_c \frac{J}{\varrho} + \int_{-\infty}^{t} \frac{4}{3}\pi\varrho_c \frac{J(t_1)}{\varrho(t_1)} \frac{dr^3(t_1)}{dt}\, dt_1. \qquad [13]$$

Introducing the surface-averaged droplet radius of Hill (1966), $\bar{r} = \sqrt{Q_2/Q_0}$, [13] is transformed into a system of four coupled differential equations:

$$\varrho \frac{dg}{dt} = 4\pi\varrho_c \left(\frac{1}{3} J r^{*3} + \varrho Q_2 \frac{d\bar{r}}{dt} \right), \qquad [14]$$

$$\varrho \frac{dQ_2}{dt} = J r^{*2} + 2\varrho Q_1 \frac{d\bar{r}}{dt}, \qquad [15]$$

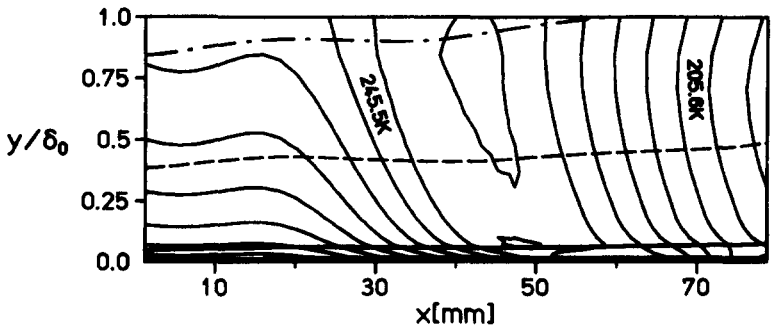

Figure 7. Diabatic temperature contours and streamlines in the sidewall boundary layer, circular-arc nozzle axis, increment $\Delta T = 5.7$ K.

$$\varrho \frac{dQ_1}{dt} = Jr^* + \varrho Q_0 \frac{d\bar{r}}{dt} \quad [16]$$

and

$$\varrho \frac{dQ_0}{dt} = J. \quad [17]$$

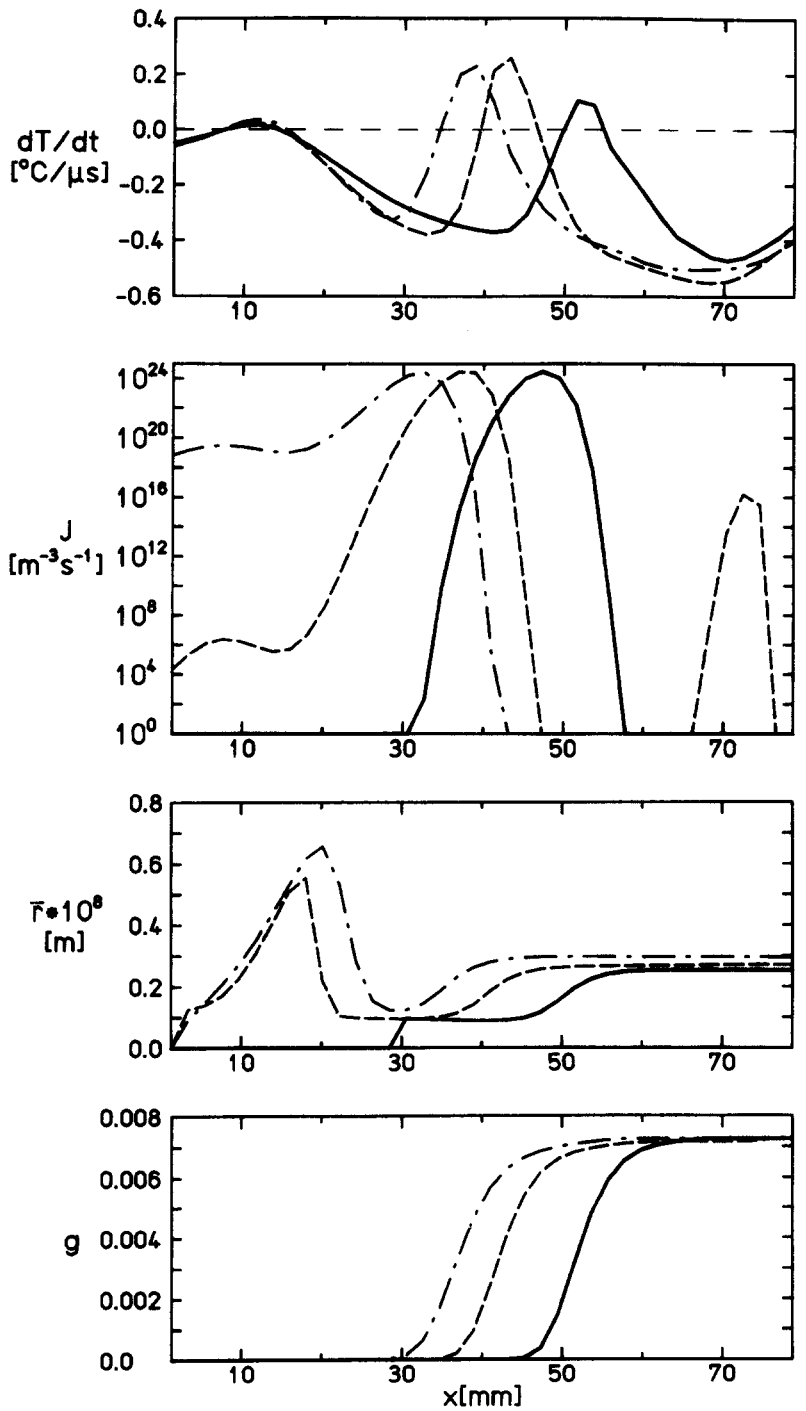

Figure 8. From the top: cooling rate dT/dt, nucleation rate J, surface-averaged droplet radius $\bar{r}$ and condensate mass fraction g along streamlines. Sidewall boundary layer, circular-arc nozzle axis: outer streamline (- - -); middle streamline (- - -); inner streamline (——).

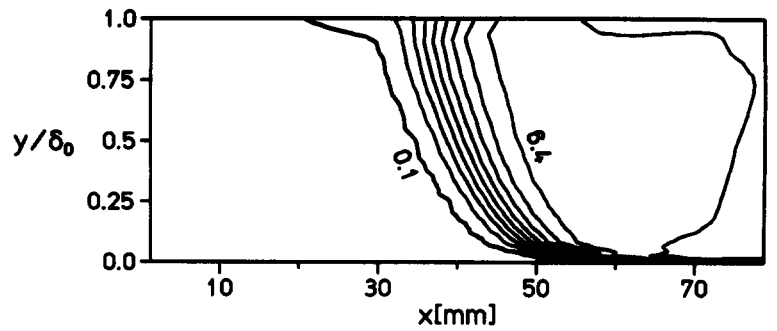

Figure 9. Condensate mass fraction contours in the boundary layer, circular-arc nozzle axis, increment $\Delta g = 0.8\ g_{cond.}/kg_{mixture}$.

Algorithm of the Method

The algorithm starts with the given static pressure distribution and the condensate mass fraction at the upper edge of the interference area taken from the 2-D inviscid diabatic calculations of Dohrmann (1989) and Schnerr & Dohrmann (1989) using a finite volume method to solve the time-dependent Euler equation. In the boundary layer the heat source distribution is estimated in the first iteration step. With the known source term on the right-hand side of [8], the analytical calculation is carried out. Then a certain number of iterations of the momentum equation follows. Thus we arrive at the state variables, the velocity distribution and the different streamlines in the boundary layer. Along these streamlines the nucleation rate and the condensate mass fraction are calculated. The heat addition by homogeneous condensation is used as an updated source term in the following iteration steps. The computation is finished when the maximum correction of the heat addition values per iteration is lower than a postulated threshold limit. The computation of the supercritical shock/boundary layer interaction with nonequilibrium phase transition requires about 80 min CPU-time on an IBM 3090 to reach a stationary solution, which is 20 times that required for the calculation of transonic turbulent boundary layers with subcritical heat addition.

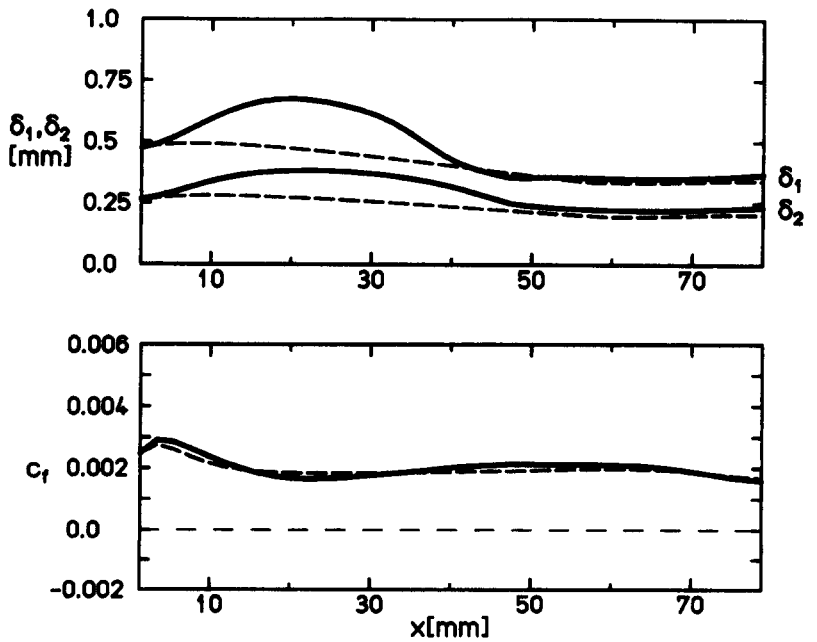

Figure 10. Adiabatic (- - -) and diabatic (——) displacement (δ_1), momentum thickness (δ_2) and friction coefficient c_f; circular-arc nozzle axis.

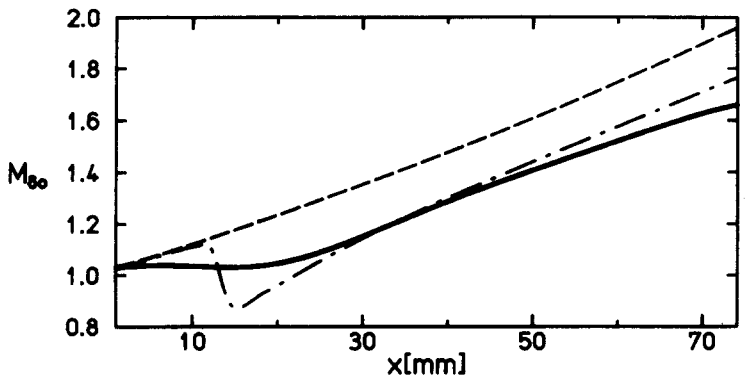

Figure 11. Adiabatic (- - -) and diabatic (——) M at the upper edge of the interference area and diabatic (- · -) M in the outer flow field; circular-arc nozzle wall.

RESULTS AND DISCUSSION

The shock/boundary layer interaction with global and local supercritical heat addition in plane Laval nozzle flow is calculated. At high relative humidities supercritical heat addition by homogeneous condensation creates a normal shock with an extended subsonic region downstream. Figure 2 shows the numerical result of Dohrmann (1989) for an inviscid circular-arc nozzle flow with the assumption of solid condensate. This nozzle has a total throat height of $2y^* = 30$ mm and a radius of curvature at the throat of 400 mm, the width is 50 mm. In this flow field the normal shock, thereby the subsonic region, stretches from the lower wall to the upper wall of the nozzle. Figure 3 shows the corresponding schlieren picture with a stationary normal shock caused by supercritical heat addition.

Figure 4 shows the adiabatic and the diabatic frozen M distributions at the upper edge of the interference area at the side wall along the nozzle axis (- - - horizontal line in figure 2). In general, $x = 0$ corresponds to the nozzle throat position. The inviscid diabatic result of Dohrmann indicates the characteristic normal shock for high rates of heat addition. After the computation of the shock/boundary layer interaction, the normal shock becomes strongly weakened near the wall and even disappears, and the acceleration afterwards is decreased (——). This is the consequence of the extended pre-compression upstream of the shock and the upper transonic limit for the onset M. The onset of heat addition at the upper edge of the interference area moves downstream compared with the inviscid result and rises to the same maximum level (figure 5). The M contours and the velocity profiles inside the boundary layer are plotted in figure 6. The velocity profiles are only moderately deformed due to the reduced pressure gradient in the main flow direction. It can be seen that the local boundary layer thickness near the outflow boundary of the interference area is smaller than that at the inflow boundary.

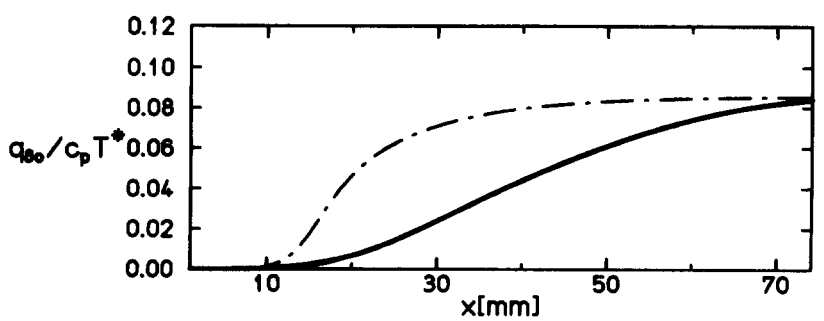

Figure 12. Heat addition from homogeneous condensation at the upper edge of the interference area (——) and in the outer flow field (- · -); circular-arc nozzle wall.

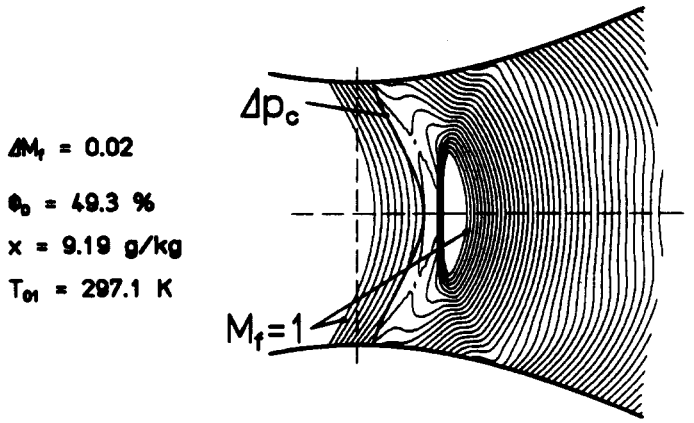

Figure 13. Local supercritical heat addition by homogeneous condensation in a hyperbolic nozzle; $2y^* = 120$ mm, $R^* = 200$ mm, temperature gradient $(dT/dx)^* = -5.54$°C/cm, frozen iso-Mach lines $M_f \geqslant 1$.

Figure 7 shows the diabatic temperature contours and three streamlines in the boundary layer. Ahead of the shock the temperature changes only moderately in the x-direction. At a fixed x-value the temperature rises with decreasing normal distance to the wall. For that reason the supersaturation diminishes and the process of nucleation and droplet growth is weakened. As a result of the latent heat release the temperature increases locally. In figure 8 the cooling rate, the nucleation rate, the surface-averaged droplet radius and the condensate mass fraction along the plotted streamlines are shown. Approaching the wall, the maxima of the cooling rate and nucleation rate are shifted downstream. At the upper and middle streamlines the surface-averaged droplet radius ($\bar{r}$) reaches a maximum upstream of the maximal nucleation rate, which is a nonphysical effect using Hill's model and has no influence on the results in the condensing area. The increase in $\bar{r}$, starting from the same level along the three streamlines with respect to the maximum nucleation rate, leads to the onset of macroscopic relevant values of the heat addition. It moves downstream approaching the wall and reaches approximately the same constant value for all three streamlines. The condensate mass fraction distribution is similar for all three streamlines but stepwise shifted downstream approaching the wall. The condensation onset is defined at the location where the condensate mass fraction reaches a level of $g_c = 0.1$ g/kg. This is shown by the first of the condensate mass fraction contours in figure 9. Inside of the boundary layer the condensation onset moves downstream with decreasing distance to the wall.

The displacement thickness (δ_1), the momentum thickness (δ_2) and the friction coefficient are compared with the corresponding values for adiabatic flow (figure 10). Both integral boundary

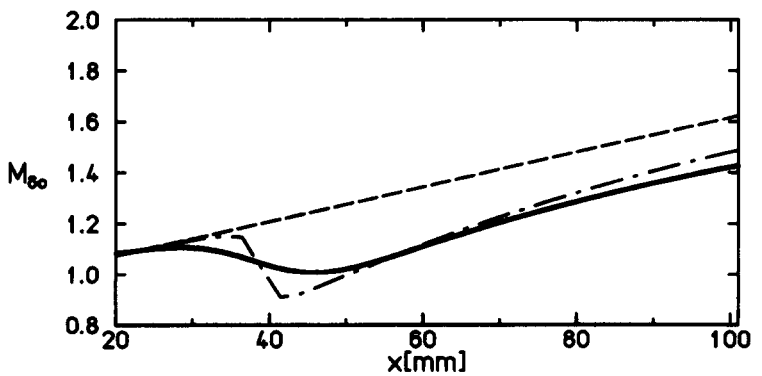

Figure 14. Adiabatic (- - -) and diabatic (——) M at the upper edge of the interference area and diabatic (- · -) M in the outer flow field; sidewall–hyperbolic nozzle axis.

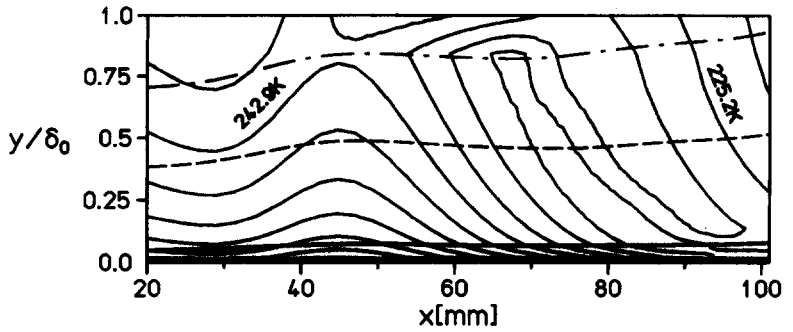

Figure 15. Diabatic temperature contours and streamlines in the sidewall boundary layer–hyperbolic nozzle axis, increment $\Delta T = 5.9$ K.

layer quantities δ_1 and δ_2 increase significantly even ahead of the normal shock by supercritical heat addition. Behind the shock they reduce to nearly the same values as those in adiabatic flow and the friction coefficient decreases only slightly.

In this slender circular-arc nozzle the inviscid flow along the sidewall at the nozzle axis is nearly identical to that at the curved nozzle wall (figure 11). Due to the shock/boundary layer interaction, the normal shock from the supercritical heat addition in the outer flow field disappears completely. The latent heat release at the upper edge of the interference area is decreased in comparison with the inviscid result (figure 12). The details of the condensation process and the integral boundary layer quantities develop similar to those in the interference region at the sidewall along the nozzle axis.

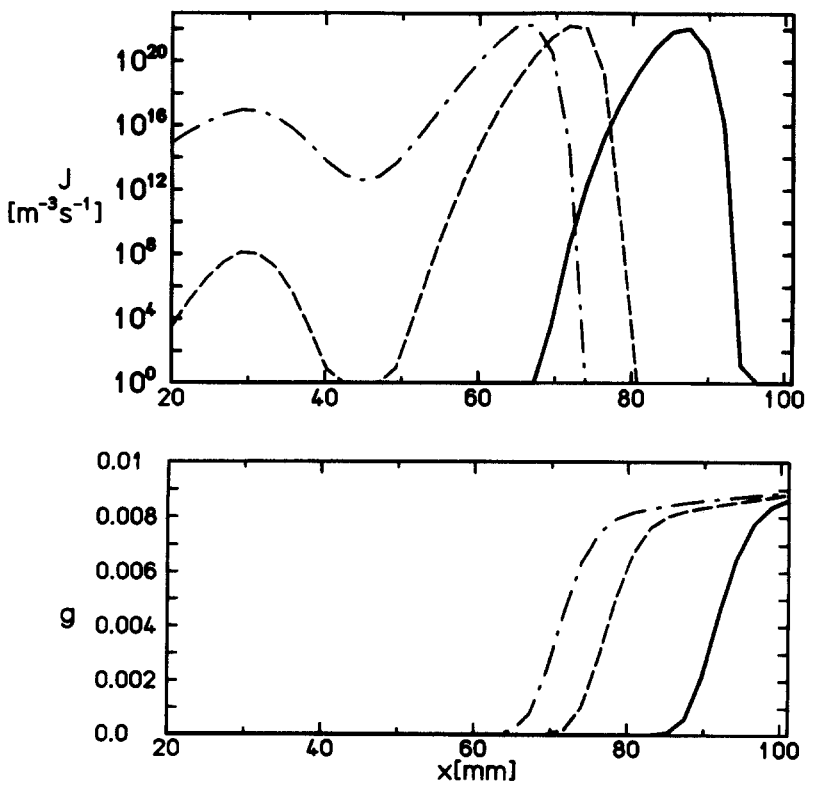

Figure 16. Nucleation rate J and condensate mass fraction g along streamlines; sidewall boundary layer–hyperbolic nozzle axis: outer streamline (- · -); middle streamline (- - -); inner streamline (——).

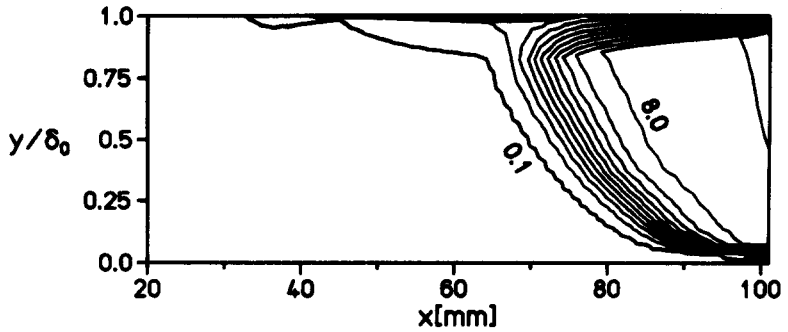

Figure 17. Condensate mass fraction contours in the boundary layer–hyperbolic nozzle axis, increment $\Delta g = 0.8\, g_{cond.}/kg_{mixture}$.

Figure 13 shows local supercritical heat addition in a hyperbolic nozzle (Dohrmann 1989) where we assume liquid condensate. In this flow the lower rates of heat addition and the higher nozzle wall curvature lead to a normal shock only in the vicinity of the nozzle axis and a continuous compression prevails at the nozzle wall. Both the strength of the inviscid shock and the resulting shock/boundary layer interaction are somewhat less than those in the previous case (figure 14). Again, the diabatic temperature contours and three streamlines in the boundary layer are depicted (figure 15), and the condensation process along these streamlines is analyzed (figure 16). The maximum nucleation rate, relevant to the condensation onset, and the condensate mass fraction distribution are also shifted downstream approaching the wall. The condensate mass fraction contours (figure 17) in the neighborhood of the boundary layer edge demonstrate a slightly different structure from that in the first example.

Figure 18 shows the adiabatic and diabatic static pressure distributions corresponding to figure 14. Because of the shock/boundary layer interaction the gradient of the pressure jump from supercritical heat addition becomes significantly weakened. Therefore, static pressure measurements by wall pressure taps may lead to misinterpretation and cannot be used for the determination of the condensation onset in condensing zones with shocks. However, in the case of subcritical heat addition the static pressure distributions at the wall and near the boundary layer edge agree completely and give the correct information about the onset of compression in the outer flow field (figure 19). In this case the measured static pressure distribution at the wall may give the correct location of the onset of macroscopic condensation effects in the inviscid domain.

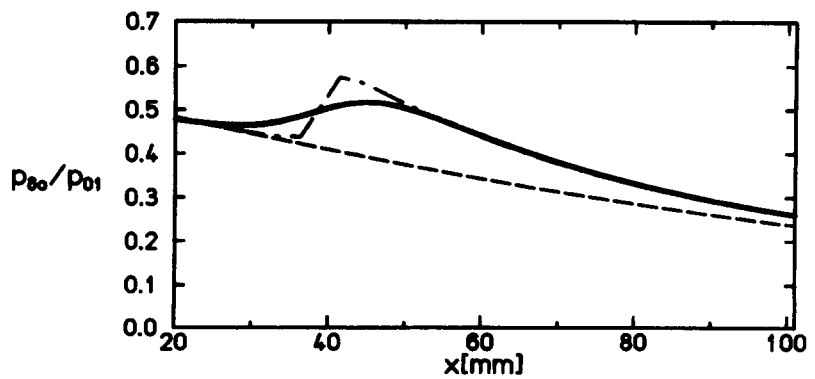

Figure 18. Supercritical heat addition—adiabatic (- - -) and diabatic (——) static pressure distributions at the upper edge of the interference area and the diabatic (- · -) one in the outer flow field; sidewall–hyperbolic nozzle axis.

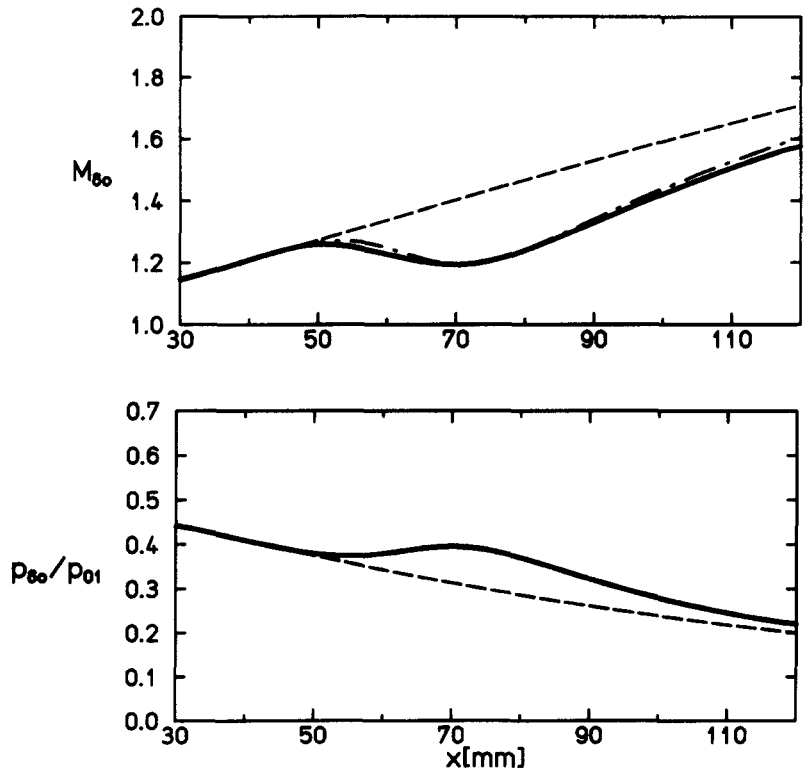

Figure 19. Subcritical heat addition—adiabatic (- - -) and diabatic M and static pressure distributions at the upper edge of the interference area (——) and in the outer flow field (- · -); sidewall–hyperbolic nozzle axis. Hyperbolic nozzle $2y^* = 120$ mm, $R^* = 200$ mm, $\phi_0 = 29.4\%$, $x = 6.68$ g/kg, $T_{01} = 300.6$ K.

CONCLUSION

The shock wave/boundary layer interaction with supercritical heat addition by homogeneous condensation is simulated by means of an analytical–numerical combination procedure. The calculation is restricted to the local shock/boundary layer interference region inside the boundary layer. The coupling with the inviscid outer flow field has not yet been considered.

Normal shocks with different strengths caused by supercritical heat addition in the outer flow field lead to somewhat varying shapes of the heating front only in the vicinity of the boundary layer edge. With decreasing distance from the wall the processes of nucleation and droplet growth are shifted downstream. In the present calculation no evaporation of condensate in a near-wall zone, due to the heat produced by friction effects, is observed. The normal shock from supercritical heat addition by homogeneous condensation causes a significant increase in the displacement and momentum thicknesses, but no separation of the boundary layer. The friction coefficients change only slightly in comparison with the values without phase transition. In the case of supercritical heat addition, the pressure measurement at the wall is difficult to interpret due to the weakening by the diabatic shock/boundary layer interaction. For subcritical heat addition the static pressure distribution at the wall indicates the correct condensation onset.

REFERENCES

BEAM, R. M. & WARMING, R. F. 1978 An implicit factored scheme for the compressible Navier–Stokes equations. *AIAA Jl* **16,** 393–402.

BOHNING, R. 1982 Die Wechselwirkung eines senkrechten Verdichtungsstoßes mit einer turbulenten Grenzschicht an einer gekrümmten Wand. Habilitationsschrift, Universität (TH) Karlsruhe, Germany.

BOHNING, R. & ZIEREP, J. 1976 Der senkrechte Verdichtungsstoß an der gekrümmten Wand unter Berücksichtigung der Reibung. *Z. Angew. Math. Phys.* **27,** 225–240.

BREITLING, T. 1989 Berechnung transsonischer, reibungsbehafteter Kanal- und Profilströmungen mit passiver Beeinflussung. Ph.D. Dissertation, Universität (TH) Karlsruhe, Germany.

CEBECI, T. & SMITH, A. M. O. 1974 Analysis of turbulent boundary layers. In *Applied Mathematics and Mechanics* (Edited by FRENKIEL, F. N. & TEMPLE, G.). *International Series of Monographs.* Academic Press, New York.

DELALE, C. F., SCHNERR, G. H. & ZIEREP, J. 1993 The mathematical theory of thermal choking in nozzle flows. *Z. Angew. Math. Phys.* **44,** 943–977.

DOHRMANN, U. 1989 Ein numerisches Verfahren zur Berechnung stationärer transsonischer Strömungen mit Energiezufuhr durch homogene Kondensation. Ph.D. Dissertation, Universität (TH) Karlsruhe, Germany.

HILL, P. G. 1966 Condensation of water vapour during supersonic expansion in nozzles. *J. Fluid Mech.* **25,** 593–620.

JANTZEN, H.-A. 1990 Theoretische und experimentelle Untersuchung zur Simulation des Kondensationsbeginns transsonischer Profilumströmungen in Lavaldüsen. Ph.D. Dissertation, Universität (TH) Karlsruhe, Germany.

LIGHTHILL, J. 1961 Interactions between normal shock waves and turbulent boundary layers. Report R&M 3262, Ames Research Center (NASA) British Aeronautical Research Council.

RYLEY, D. J. 1971 The behaviour of nucleation fogs within the nozzle boundary layers in the wet steam turbine. *J. Mech. Engng Sci.* **13,** 190–199.

SCHNERR, G. H. 1986 Homogene Kondensation in stationären transsonischen Strömungen durch Lavaldüsen und um Profile. Habilitationsschrift, Universität (TH) Karlsruhe, Germany.

SCHNERR, G. H. 1989 2-D transonic flow with energy supply by homogeneous condensation: onset condition and 2-D structure of steady Laval nozzle flow. *Expts Fluids* **7,** 145–156.

SCHNERR, G. H. 1993 Transonic aerodynamics including strong effects from heat addition. *Computers Fluids* **22,** 103–116.

SCHNERR, G. H. & DOHRMANN, U. 1989 Ein numerisches Verfahren zur Berechnung stationärer transsonischer Strömungen mit Relaxation und Wärmezufuhr. *Z. Angew. Math. Mech.* **69,** 588–591.

SCHNERR, G. H. & DOHRMANN, U. 1990 Transonic flow around airfoils with relaxation and energy supply by homogeneous condensation. *AIAA Jl* **28,** 1187–1193. See also AIAA Paper 89-1834, presented at the *20th Fluid Dynamics, Plasma Dynamics and Lasers Conf.*, Buffalo, NY (June 1989).

SCHNERR, G. H., BOHNING, R., BREITLING, T. & JANTZEN, H.-A. 1992 Compressible turbulent boundary layers with heat addition by homogeneous condensation. *AIAA Jl* **30,** 1284–1289.

STUDZINSKY, W. 1979 Boundary layer in compressible flow of wet water vapour. *Int. J. Multiphase Flow* **5,** 185–199.

VOLMER, M. 1939 *Kinetik der Phasenbildung.* Steinkopf, Leipzig, Germany.

WEGENER, P. P. 1987 Nucleation of nitrogen: experiment and theory. *J. Phys. Chem.* **91,** 2479–2481.

WEGENER, P. P. 1991 Cryogenic wind tunnels and the condensation of nitrogen. *Expts Fluids* **11,** 333–338.

ZIEREP, J. 1971 Similarity laws and modeling. In *Gasdynamics Series of Monographs* (Edited by WEGENER, P. P.). Marcel Dekker, New York.

ZIEREP, J. 1974 Theory of flows in compressible media with heat addition. AGARDograph No. 191.